International Journal of Scientific World, 3 (2) (2015) 227-238
www.sciencepubco.com/index.php/IJSW
©Science Publishing Corporation
doi: 10.14419/ijsw.v3i2.4881
Review Paper

Analytical and simulation results of micro-ring resonator system using two eyes imaging model

C. Tanaram [1]*, P. Phatharacorn [2], S. Chiangga [2], P.P. Yupapin [1, 2]

[1] *Interdisciplinary Research Center, Faculty of Science and Technology, Kasem Bundit University, Bangkok 10250, Thailand*
[2] *Spintronics Research Center, Department of Physics, Faculty of Science, Kasetsart University, Bangkok 10900, Thailand*
**Corresponding author E-mail: kypreech@kmitl.ac.th*

Copyright © 2015 C. Tanaram et al. This is an open access article distributed under the Creative Commons Attribution License, which permits unrestricted use, distribution, and reproduction in any medium, provided the original work is properly cited.

Abstract

In this review article, the artificial vision model using the 3 cascaded conjugate mirrors system can be constructed, analyzed and simulated. A single 3D pixel (point) imaging construction is formed and obtained by using the conjugate mirror concept, where the large area of pixels can be potentially constructed and realized for large area application. This is a simulation work, where the software program is the finite difference time domain (FDTD) commercial program (Opti-wave). However, the used device parameters and materials can be fabricated and formed the artificial eyes for 3D artificial vision. Simulation result obtained has shown that the whispering gallery modes (WGMs) of radiation within the cascaded microring conjugate mirrors can be easily formed, and are coupled by the two nonlinear side rings, which can be potentially used for 3D imaging pixel construction applications by the two eyes construction model.

Keywords: *Micro-Conjugate Mirror; 3D Image Construction; Artificial Vision Model, Artificial Eye Model, 3D Imaging Pixel, Artificial Organs.*

1. Introduction

Most of the important artificial eye research issues are to give the blind person sight ability, which normally use the bionic eyes and depend on the circumstances surrounding the loss of sight. Retinal prostheses are the most prevalent visual prosthetic under developments, which they are the candidates for visual prosthetic implants find the procedure most successful if the optic nerves were developed prior to the onset of blindness. The visual prosthetics have been developed as a potentially valuable aid for visual individual degradation, where all other efforts remain investigation. Artificial eyes have become the important instruments for various applications [1-3] and the potential applications have been demonstrated [4-6]. One aspect of results has shown the feasibility of using artificial eyes for human eye replacement [7, 8] that the possibility of vision image connection between optic nerve and brain cells is useful for realistic artificial eye can be realized [9]. The use of THz technology can be adopted to employ with human tissue penetration and investigation, where there are many research reported for imaging and investigations [10, 11]. The interesting result of whispering gallery mode (WGM) of light within a tiny optical device to generate the 3D image basic device known as a conjugate mirror can be easily constructed by using the WGMs of light within a PANDA ring circuit[12, 13]. The WGMs with THz frequency range can be generated and used to form the 3D image and linked to the optic nerves in human brain [14]. The artificial eyes can be constructed, which has currently become the current challenge researches and investigations.

Humanoid robot has become the best robotic type in robotic technology, which there are required many components and related technologies. Robotic research and development has been the important issue of the world robotic society for years [15-19], where the main part of robotic components is the process for brain communication and commands. To obtain the realistic robotic brain and its functions, the brains signal and communications are required to manipulate and test [20-24], therefore, the searching of realized technique for brain signals remains. In applications, especially, in bioengineering, THz signals have been involved in many applications [25-28], particularly, in medical applications [29, 30]. THz is applied to electromagnetic radiation with the high-frequency edge of the millimeter wave band, 300 GHz (0.3 THz), and the low frequency edge of the far-infrared light band, 3,000 GHz (3THz). Corresponding wavelengths of

radiation in this band range are from 1 mm to 0.1 mm (or 100 μm). THz radiation consists of electromagnetic waves with frequency between 0.1 THz to 10 THz, and is widespread biomedical application involving the interaction of terahertz pulse with biological media[31-36], where THz radiation has been used successfully as a noninvasive imaging technique for detection of human skin cancer [37, 38]. Recently, Yupapin et al have shown the interesting results of whispering gallery mode of light within a PANDA ring circuit[13, 14], in which the advantage is that the WGMs can be easily generated and controlled within the PANDA ring circuit, which can be useful for various applications. The other applications of Panda ring resonator can be found in references [39-46].

In this article, we have proposed a simulation work of 3D imaging based on the two eyes construction model, however, the device parameters and material can be fabricated and formed such a proposed system for 3D artificial vision. The 3D image can be formed by using the conjugate mirrors, and the artificial eye model is discussed. In simulation, the partially reflected light intensities from two device ends are interfered and the 3D whispering gallery modes within the small ring constructed by four-wave mixing of waves. The 3D image (pixel) can be linked to the optic nerve (optic chiasm), the scanning image for large area is also available, where finally the 3D images can be constructed and linked to the human perceptions. This article is extension of the previous published papers [47, 48], in which basic details and more simulation results of artificial eyes using a PANDA ring conjugate mirror is formed by resonator as a foundation, which can be a useful resource for readers in many areas of applications. In practice, when the realistic device parameters are used, such a device can be fabricated and implemented, especially, for artificial eyes and spying investigation works, which can therefore be available for various works in the near future.

2. Analytical

Light from the laser source which is a monochromatic light source is input into the PANDA ring waveguide via the input port, which is in the form of phase modulation input, which is shown in Figure 1, the Gaussian pulse [49] is given by

$$E_{in_1} = E(z = 0, x) = A_0 e^{-\frac{x^2}{2w^2}} \tag{1}$$

Where w, A_0 are constants of Gaussian signal and define electric field each point on the ring, where in case of a single input, $E_{in_2} = E_{Add} = 0$, the following fields are expressed by [50]

$$E_1 = \frac{j\sqrt{1-\gamma_1}\sqrt{\kappa_1}}{1-\sqrt{1-\gamma_1}\sqrt{1-\kappa_1}\, e^{-\frac{\alpha}{2}L - jk_nL}} E_i \,,\; E_4 = \frac{j\sqrt{1-\gamma_1}\sqrt{\kappa_1}\, e^{-\frac{\alpha}{2}L - jk_nL}}{1-\sqrt{1-\gamma_1}\sqrt{1-\kappa_1}\, e^{-\frac{\alpha}{2}L - jk_nL}} E_i$$

$$E_2 = \left[\frac{\sqrt{1-\gamma_3}\sqrt{1-\kappa_3} - (1-\gamma_3)\, e^{-\frac{\alpha}{2}L_2 - Jk_nL_2}}{1-\sqrt{1-\gamma_3}\sqrt{1-\kappa_3}\, e^{-\frac{\alpha}{2}L_2 - Jk_nL_2}}\right] e^{\frac{\alpha L}{22} - jk_n\frac{L}{2}} E_1,\; E_3 = \sqrt{1-\gamma_2}\sqrt{1-\kappa_2}\left[\frac{\sqrt{1-\gamma_3}\sqrt{1-\kappa_3} - (1-\gamma_3)\, e^{-\frac{\alpha}{2}L_2 - jk_nL_2}}{1-\sqrt{1-\gamma_3}\sqrt{1-\kappa_3}\, e^{-\frac{\alpha}{2}L_2 - jk_nL_2}}\right] e^{\frac{\alpha L}{22} - jk_n\frac{L}{2}} E_1$$

where E_1, E_2, E_3, E_4 are the electric fields, $\gamma_1, \gamma_2, \gamma_3, \gamma_4$ are the fractional coupler intensity losses, $\kappa_1, \kappa_2, \kappa_3, \kappa_4$ are the coupling coefficients, α is an attenuation coefficient, $k_n = \frac{2\pi}{\lambda}$ is the wave propagation number in vacuum, $L = 2\pi R$ is the center ring propagation distance, $L_2 = 2\pi R_2$ is the small ring(side ring) propagation distance, $j = \sqrt{-1}$ is the imaginary part of complex number, and the refractive index of the substances used in the system is defined by [50]

$$n = n_0 + n_2 I = n_0 + \left(\frac{n_2}{A_{eff}}\right) P \tag{2}$$

Where n_0, n_2 are the linear and nonlinear refractive indices, I and Pare the optical intensity and power, respectively. A_{eff} Is the effective mode core area [51], which is ranged between 0.10 and 0.50 μm^2. The optical phase (φ) is given by

$$\phi(t) = \phi_0 + \phi_{NL} = \phi_0 + \frac{2\pi n_2}{A_{eff}} L|E_0(t)|^2 \tag{3}$$

Where ϕ_0 represents the linear optical phase, ϕ_{NL} is the nonlinear optical phase, L is a circumference of PANDA ring and $|E_0(t)|^2$ is the optical intensity.

By configuring the input fields within the PANDA ring, in which $E_{i_1} = E_i$, $E_{in_2} = E_{Add} = 0$. The Maxwell's equations [52] within the device (waveguide) can be written in the form of Helmholtz's wave equations as [53]

$$\nabla^2\vec{E}(\rho, \phi, z) + k^2\vec{E}(\rho, \phi, z) = 0 \tag{4}$$

$$\frac{\partial^2 E(\rho, \phi, z)}{\partial \rho^2} + \frac{1}{\rho}\frac{\partial E(\rho, \phi, z)}{\partial \rho} + \frac{1}{\rho^2}\frac{\partial^2 E(\rho, \phi, z)}{\partial \phi^2} + \frac{\partial^2 E(\rho, \phi, z)}{\partial z^2} + k^2 \vec{E}(\rho, \phi, z) = 0 \quad (5)$$

By using separation variables in cylindrical coordinates [54], the solution of the Helmholtz equation of equations (4) and (5) is given by equation (6).

$$E(\rho, \phi, z) = R(\rho)\Phi(\phi)Z(z) \quad (6)$$

In the case of $\rho < a$, we obtain

$$R_i(\rho) = C_m J(k_i \rho) \quad (7a)$$

The solution of equation (4) is written as

$$\Phi(\phi) = A_m \cos(m\phi) \quad m = 1,2,3,4,\ldots \quad (7b)$$

When the ring thickness is H, we obtain

$$Z(z) = \sinh(kz) \quad (7c)$$

The electric fields are obtained by the following equation

$$E_{zm}(\rho, \phi, z) = \sum_{m=0}^{\infty} \sum_{n=1}^{\infty} A_m C_m J_m(k_{mn}\rho) \cos(m\phi) = B_m J(k_i \rho) \cos(m\theta) \quad (8)$$

When $A_m C_m = B_m$, the boundary conditions are given by equation (9)

$$\rho = 0 \text{ , } D = 0 \qquad R_o(a) = R_i(a) \quad (9a)$$

$$\rho = a \qquad \frac{dR_o(a)}{d\rho} = \frac{dR_i(a)}{d\rho} \quad (9b)$$

When the system is in the WGM condition, the optimum output can be obtained by equation (10).

$$\frac{\partial E_1(\rho,\phi)}{\partial \rho} = 0, \qquad \text{when} \qquad \rho < a \quad (10)$$

From the condition that $J'_m(k\rho) = 0$, the current relation is obtained [55], where in this case the single Panda ring output is used as the device.

$$k\rho J_{m-1}(k\rho) - mJ_m(k\rho) = 0 \quad (11)$$

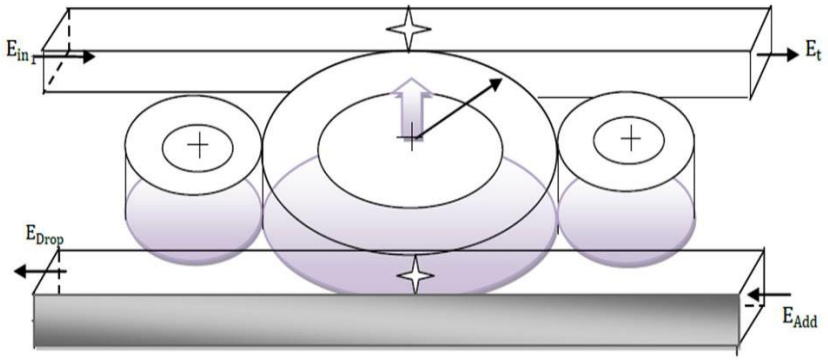


Fig. 1: A Schematic of a PANDA ring resonator, where E_{in}: Input port optical field, E_t: Through port output field, E_{drop}: Drop port output field, E_{add}: Add port input field.

3. Simulation

In simulation, the WGM output can be obtained by using equation (12). After the Gaussian pulse is input into the system via input port as shown in Figure 1 [56], the resonant WGM output is obtained when the differentiation of WGM field at the ring center is vanished, the input is given by

$$E_{in} = \frac{wA_0}{(w^2 + j\frac{z}{k_0 n_0})^{\frac{1}{2}}} \exp\left[- \frac{x^2}{2(w^2 + j\frac{z}{k_0 n_0})} \right] \tag{12}$$

For convenience, the polar coordinates are used to calculate the value of E_1, the results are expressed by

$$E_1(z, x) = \left(\frac{j\sqrt{1 - \gamma_1}\sqrt{\kappa_1}}{1 - \sqrt{1 - \gamma_1}\sqrt{1 - \kappa_1} e^{-\frac{\alpha}{2}L - jk_n L}} \right) \left(\frac{wA_0}{\left(w^2 + j\frac{z}{k_0 n_0}\right)^{\frac{1}{2}}} \right) \exp\left[- \frac{w^2 x^2}{2\left(w^4 - \frac{z^2}{k_0^2 n_0^2}\right)} + j\left(k_0 n_0 + \frac{x^2}{2k_0 n_0 \left(w^4 - \frac{z^2}{k_0^2 n_0^2}\right)} \right) z \right] \tag{13}$$

The polar coordinate system of $E_1(z, x)$ is $E_1(\rho, \phi)$, which is expressed by.

$$|E_1(\rho, \phi)| = \frac{x_1\sqrt{\kappa_1}}{\left(1 - 2x_1 x_2 e^{-\frac{\alpha}{2}L} \cos k_n L + e^{-\alpha L} x_1^2 y_1^2\right)^{\frac{1}{2}}} \left(\frac{wA_0}{\left(w^4 + \frac{\rho^2\phi^2}{k_0^2 n_0^2}\right)^{\frac{1}{2}}} \right) \exp\left[- \frac{w^2 k_{mn}^2 \rho^2}{2\left(w^4 - \frac{\rho^2\phi^2}{k_0^2 n_0^2}\right)} \right] \tag{14}$$

Substitute equation (14) into Fourier-Bessel series [57], the solution of equation (7b) is B_{mn} and given by

$$B_{mn} = \frac{2\text{cosech}(k_{mn}L)}{\pi a^2 J_{m+1}^2(k_{mn}a)} \int_0^{2\pi} d\phi \int_0^a \rho E_1(\rho,\phi) J_m(k_{mn}\rho)\cos(m\phi) d\rho \tag{15}$$

Where $L = \pi a/2$ is the arc length of PANDA ring, the electric field equation (8) is written as

$$E_1(\rho, \phi) = \frac{4\pi\text{cosech}(k_{mn}L) J_m(k_{mn}\rho)\cos^2 m\phi}{\pi a^2 J_{m+1}^2(k_{mn}a)} \left[\frac{x_1\sqrt{\kappa_1}}{\left(1 - 2x_1 y_1 e^{-\frac{\alpha}{2}L} \cos k_n L + e^{-\alpha L} x_1^2 y_1^2\right)^{\frac{1}{2}}} \right] \times$$

$$\times \frac{(wA_0)(k_0 n_0)^{\frac{1}{2}}}{B^{\frac{1}{4}}} \int_0^a J_m(k_{mn}\rho) \left[\rho - \left(\frac{A}{2(B + C\rho^2)} + \frac{1}{4}\frac{C}{B} \right) \rho^3 \right] d\rho \tag{16}$$

Give $A = k_{mn}^2 k_0^2 w^2 n_0^2 \rho^2$, $B = w^4 k_0^2 n_0^2$, $C = \phi^2$

$$\int_0^a J_m(k_{mn}\rho) \left[\rho - \left(\frac{A}{2(B + C\rho^2)} + \frac{1}{4}\frac{C}{B} \right) \rho^3 \right] d\rho \cong - \frac{2\rho^2}{k_{0n}^2} \left(\frac{A}{2(B + C\rho^2)} + \frac{1}{4}\frac{C}{B} \right) J_0(k_{0n}\rho) +$$

$$+ \left[\frac{\rho}{k_{0n}} - \frac{\rho^3}{k_{0n}} \left(\frac{A}{2(B + C\rho^2)} + \frac{1}{4}\frac{C}{B} \right) + \frac{4\rho}{k_{0n}^3} \left(\frac{A}{2(B + C\rho^2)} + \frac{1}{4}\frac{C}{B} \right) \right] J_1(k_{0n}\rho) \tag{17}$$

The solution of equation (17) is given by (18), which is a cubic equation. Then, the result in equation (16) is the $E_1(\rho, \phi)$ of the PANDA ring. From equation (10), consider the integral Bessel function [58] in equation (16), which is the WGM from the estimation of equation (18) in terms of an equation cubic equation (by approximately a third term in Taylor's series) as follows. The solution of ρ is expressed by

$$1 - \left[\frac{A}{2B} + \frac{1}{4}\frac{C}{B} + \frac{3k_{0n}^2}{4} \right] z$$

$$+ \left[\begin{array}{c} \frac{3Ak_{0n}^2}{8B} \\ + \frac{3k_{0n}^2}{16}\frac{C}{B} \\ + \frac{3k_{0n}^4}{32} \end{array} \right]$$

$$z^2 - \left[\left(\begin{matrix}\frac{Ak_{0n}^4}{16B} \\ + \frac{k_{0n}^4}{32}\frac{C}{B}\end{matrix}\right)\right] z^3 = 0 \quad (18)$$

Solve the cubic equation by using the equation (19), where the cubic equation is given by

$$az^3 + bz^2 + cz + d = 0$$

$$a = \left[\begin{matrix}-\frac{Ak_{0n}^4}{16B} \\ -\frac{k_{0n}^4}{32}\frac{C}{B}\end{matrix}\right],$$

$$b = \left[\begin{matrix}\frac{3Ak_{0n}^2}{8B} \\ +\frac{3k_{0n}^2}{16}\frac{C}{B} \\ +\frac{3k_{0n}^4}{32}\end{matrix}\right],$$

$$c = \left[-\frac{A}{2B} - \frac{1}{4}\frac{C}{B} - \frac{3k_{0n}^2}{4}\right], \quad d = 1$$

The solution of cubic equation is defined to be

$$p = -\frac{b}{3a}, \quad q = p^3 + \frac{(bc - 3ad)}{6a^2}, \quad r = \frac{c}{3a}$$

$$\rho = \sqrt{z} = \sqrt{[q + (q^2+((r - p^2)^3)^{\frac{1}{2}}]^{\frac{1}{3}} + [q - (q^2+((r - p^2)^3)^{\frac{1}{2}}]^{\frac{1}{3}} + p} \quad (19)$$

Which was first published by Cardano in 1545 [59]

$$L = \frac{\pi a}{2}, \quad x_1 = \sqrt{1 - \gamma_1}, \quad y_1 = \sqrt{1 - \kappa_1}, \quad k_0 = \frac{2\pi}{\lambda_0} n_{eff}$$

Where n_0 is a linear reflective index, A_0 is an input field amplitude, L is a ring circumference, n_{eff} effective of reflective index in equation (2), and λ_0 wavelength in PANDA ring system.
The WGM is obtained by using the condition in equation (20)

$$\frac{\partial E_1(\rho,\phi)}{\partial \rho} = 0 \quad \text{at} \quad m = 0 \quad (20)$$

Substitute equation (19) into equation (16), we obtain

$$E_{max}(\rho,\phi) = \frac{4\,\text{cosech}\left(k_{0n}\frac{\pi a}{2}\right)}{a^2 J_1^2(k_{0n}a)} \left[\frac{x_1\sqrt{\kappa_1}}{\left(1 - 2x_1y_1 e^{-\frac{\alpha_1}{2}L}\cos k_n L + e^{-\alpha L}x_1^2 y_1^2\right)^{\frac{1}{2}}}\right] \times$$

$$\times \frac{(wA_0)(k_0n_0)^{\frac{1}{2}}}{B^{\frac{1}{4}}} J_0(k_{0n}\rho) \int_0^a J_0(k_{0n}\rho)\left[\rho - \left(\frac{A}{2(B + C\rho^2)} + \frac{1}{4}\frac{C}{B}\right)\rho^3\right] d\rho \quad (21)$$

Substitute a value of $E_{max}(\rho, \phi)$ into equation (21) with all possible waves around, in which the result should be multiplied by N the equation below.

$$E_n(\rho,\phi) = g\{E_1(\rho,\phi)\} \quad (22)$$

Where the propagation time can be configured by number of cycle, which can be about 10,000 to 20,000 round-trips before the system to optimum and stable conditions being achieved

Three study cases are performed in this work, where the first experimental results use Opti-wave finite difference time domain (FDTD) method to present optical wave propagation along the waveguide. Secondly, the mathematical simulation results are obtained by using the MATLAB program, which is shown consistently with the first experimental results. The final experimental result is obtained using the Opti-wave program, in which the terms of equation (21) is $2\pi a \cong \frac{m\lambda_0}{n_i}$ [60].

In the first simulation data, the given parameters are mode m = 0, N = 20,000, $A_{eff} = 0.3\ \mu m^2$, $\lambda_0 = 1.79\ \mu m$. The device dimensions is 20.0 μm (length) × 10.0 μm (width), where

$$|E_{in}(z, x)| = \frac{wA_0}{(w^4 + \frac{z^2}{k_0^2 n_0^2})^{\frac{1}{4}}} \exp\left[-\frac{w^2x^2}{2(w^4 + \frac{z^2}{k_0^2 n_0^2})}\right] \quad (23)$$

and

$$|E_{in}(z, x)|^2 = \frac{w^2A_0^2}{(w^4 + \frac{z^2}{k_0^2 n_0^2})^{\frac{1}{2}}} \exp\left[-\frac{w^2x^2}{w^4 + \frac{z^2}{k_0^2 n_0^2}}\right] \quad (24)$$

Where w, A_0 are constants, $k_0 = \frac{2\pi}{\lambda_0} n_{eff}$, $n_{eff} = 3.14$, $\lambda_0 = 1{,}550$ nm, $k_0 = \frac{\omega}{c} = \frac{2\pi f}{c}$ is the propagation constant in vacuum, when z and x are the dimensions along and transverse to the waveguide. The effect of a given input is calculated by using the Optic-wave program compared with the mathematical model in equation (12), where the obtained results are shown in Table 1. The second simulation data is obtained and shown in Table 2, where the given parameters are mode m = 0, N = 20,000, $A_{eff} = 0.3\ \mu m^2$, $\lambda_0 = 1.79\ \mu m$. The obtained results are compared with the calculation by using equation (16), where

Rad= a = 3.56 μm, $R_1 = R_2 = 1.23\ \mu m$, $n_{eff} = 3.14$, $n_2 = 1.3\times 10^{-13} cm^2/W$, $\kappa_1 = \kappa_2 = \kappa_3 = \kappa_4 = 0.5$.

Table 1: Results of Output Intensities at Wavelength 1.792 "μm" , P =0.1 W and "R" _"Ad" " =" 3.5 μm [61], "M = 0" Using Equations (12), (23) and (24)

Z (μm)	$\|E_{in}(z, x)\|$ Equation (12)	$\|E_{in}(z, x)\|$ V/m From FDTD	Electric field Intensity $\|E_{in}(z, x)\|^2$ Equation (12)×10^3	Electric field Intensity $\|E_{in}(z, x)\|^2$ FDTD ×10^3
0.0	49.9979	55.85	2,500.00	3,119.22
0.5	49.9979	58.77	2,500.00	3,453.91
1.0	49.9998	58.10	2,500.00	3,375.61
1.5	49.9998	53.81	2,500.00	2,895.52
2.0	49.9999	55.32	2,500.00	3,060.30
2.5	49.9997	55.48	2,500.00	3,078.03
3.0	49.9996	55.91	2,500.00	3,125.93
3.5	49.9995	56.09	2,500.00	3,146.09
4.0	49.9995	59.71	2,500.00	3,565.28
4.5	49.9994	55.48	2,499.99	3,078.03
5.0	49.9992	52.57	2,499.99	2,763.60

In this work, the required key condition is the optimum WGM output distribution, which can be controlled by ring and input laser source parameters. In simulation, the practical device parameters are given for InGaAsP/InP, where the ring parameters are mode m = 0, N = 20,000, $A_{eff} = 0.3\ \mu m^2$, $\lambda_0 = 1.79\ \mu m$, where the other ring parameters are Rad = a = 3.56 μm, $R_1 = R_2 = 1.22\ \mu m$, $n_{eff} = 3.14$, $n_2 = 1.3\times 10^{-13}\ cm^2/W$, $\kappa_1 = \kappa_2 = \kappa_3 = \kappa_4 = 0.5$. By using the given parameters, some results are calculated and obtained. Results of output intensity at wavelength 1.79 μm were calculated and obtained as shown in Table 1, where P =0.1 W, $R_{ad} = 3.5\ \mu m$, m = 0 were calculated by using equations (12), (23) and (24). In Table 2, results of output intensities using equation (16) were calculated and obtained, which they are the results of a PANDA ring circuit at wavelength 1.79 μm, $R_{ad} = 1.22\ \mu m$ m = 0. The cubic equation coefficient values in Table 3 were obtained by using equations (18) and (19). Results for the maximum

PANDA ring WGM outputs are as shown in Table 4. The resonant wavelengths of a PANDA ring resonator using equation (19) are shown in Table 5. Figure 2 shows the simulation results of WGM in a PANDA ring, where (a) PANDA ring radius is 3 μm, the left-right ring radii are 1.125 μm, (b) the WGM output of waveguide at wavelength 1.29 μm, (c) the through port signal and (d) the drop port signal at frequency between 1-500 THz. Figure 3 shows the simulation results of WGM in a PANDA ring, where (a) PANDA ring radius is 3.5 μm, the left-right ring radii are 1.22 μm, (b) the WGM output of waveguide at wavelength 1.79 μm, (c) the through port signal and (d) the drop port signal at frequency between 1-300 THz. Figure 4 shows the two-dimension whispering gallery mode of light within a PANDA ring waveguide InGaAsP/InP, where (a) PANDA is 4.5 μm, the left-right ring radii are 1.55 μm, (b) the WGM output of waveguide at wavelength 1.89 μm, (c) the through port signal, (d) the drop port signal at frequency between 1-300 THz.

Table 2: Results of output intensities using equation (16), which are the results in a PANDA ring with wavelength 1.7925 μm, R_{Ad} = 1.225 μm, mode of electromagnetic field Is M = 0

ϕ (Radian)	$\lvert E_1(\rho, \phi)\rvert$ Equation (16)	$\lvert E_1(\rho, \phi)\rvert$ From FDTD	$\lvert E_1(\rho, \phi)\rvert^2$ Equation (16)$\times 10^3$	$\lvert E_1(\rho, \phi)\rvert^2$ FDTD $\times 10^3$
0	63.1584	63.36	3,988.98	4,014.49
$\pi/6$	66.5878	59.46	4,433.94	3,535.49
$\pi/4$	70.8744	69.48	5,023.18	4,827.47
$\pi/3$	76.8758	62.18	5,909.89	3,866.35
$\pi/2$	94.0224	63.69	8,840.21	4,056.42

Table 3: The cubic equation coefficient values obtained by using equations (18) and (19)

Phase ϕ (Radian)	Cubic equation coefficients				Radius of PANDA ring Roots of cubic equation		
	a	b	c	d			
0	-4.273338071	1686.653374	-136.9343183	1.0	616.6973	0.073	0.0081
0.274376392	-4.273339412	1686.653382	-136.9343612	1.0	616.6240	0.073	0.0081
0.617346883	-4.273341088	1686.653392	-136.9344148	1.0	616.6137	0.073	0.0081
1.097505569	-4.273343434	1686.653406	-136.9344889	1.0	616.6144	0.073	0.0081
2.469387531	-4.273350138	1686.653447	-136.9347044	1.0	616.6125	0.073	0.0081

Table 4: Results for the maximum PANDA ring WGM outputs

Phase ϕ (Radians)	$E_{max}(\rho, \phi)$ Result from calculation	Result from Opti-wave
0	60,4418	63.36
0.274376392	60.4411	59.46
0.617346883	60.4402	69.48
1.097505569	60.4389	62.18
2.469387531	60.4354	63.69

Table 5: Results of the resonant wavelengths of a PANDA ring resonator using equation (19) [62].

Mode (m)	Resonant wavelength (nm)	FSR(nm)
1	2099.4385	353.2959
2	1746.1426	248.6634
3	1497.4792	184.5153
4	1312.9639	142.4164
5	1170.5475	113.2828

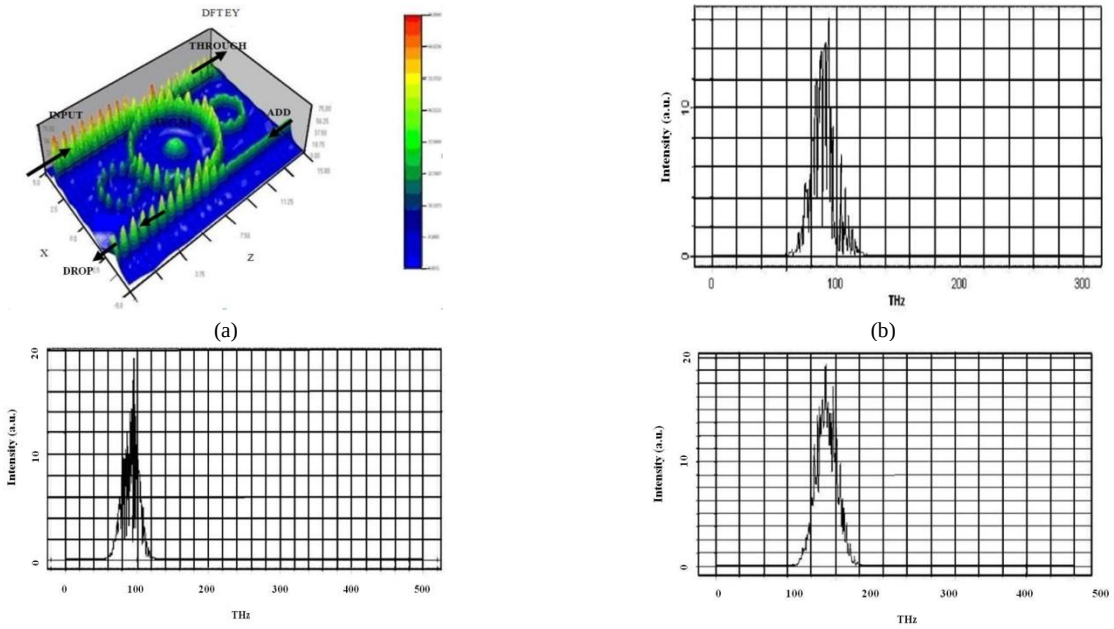


Fig. 2: Simulation results of WGM in a PANDA ring, where (a) PANDA ring radius is 3.0 µm; the left-right ring radii are 1.125 µm, (b) WGM output with wavelength 1.292 µm, (c) the Through port signal and (d) the Drop port signal with Frequency between 1-500 THz.

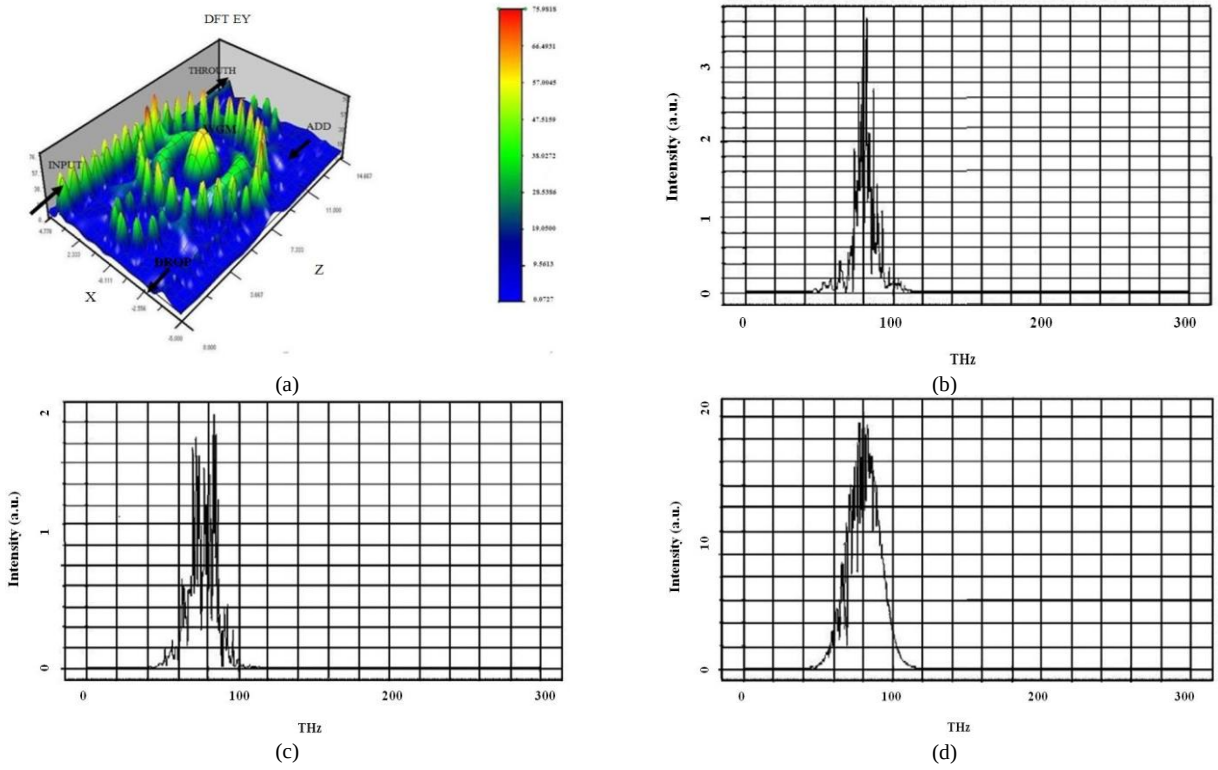


Fig. 3: Simulation results of WGM in a PANDA ring, where (a) PANDA ring radius is 3.5 µm, the left-right ring radii are 1.225 µm, (b) the WGM output of waveguide with wavelength 1.7925 µm, (c) the Through port signal and (d) the Drop port signal with frequency between 1-300 THz.

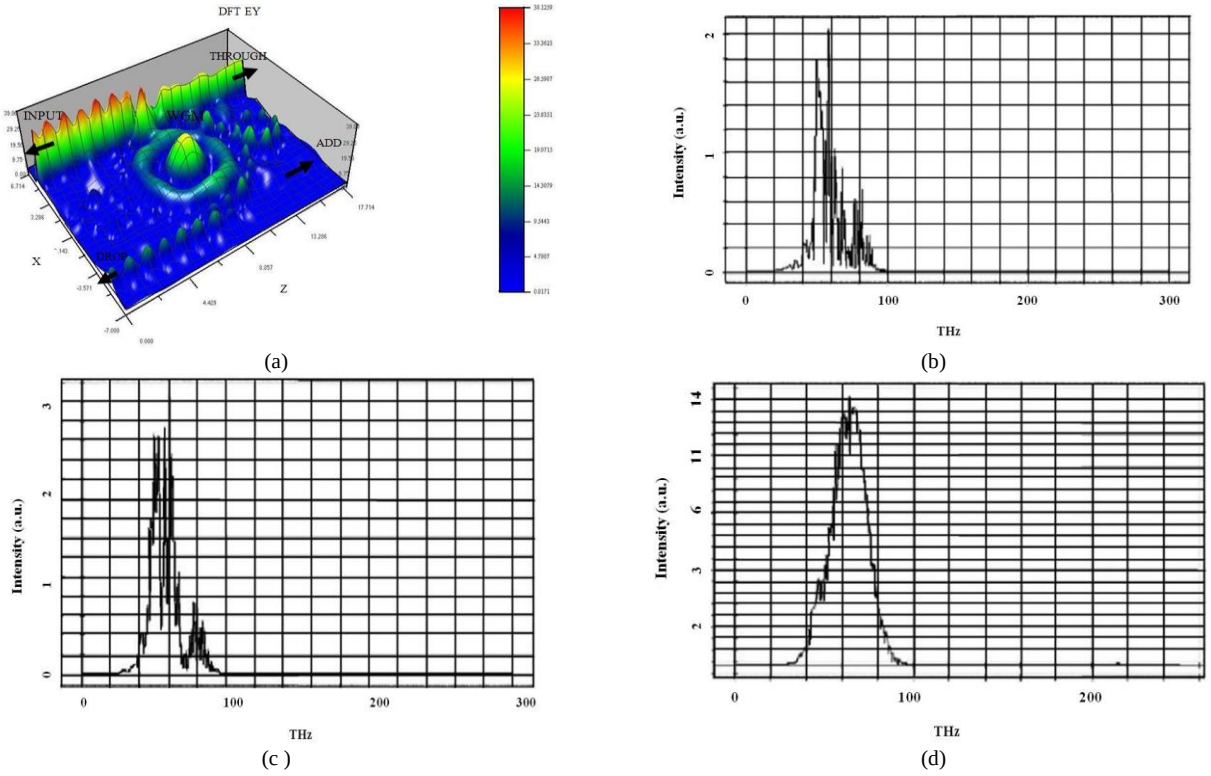


Fig. 4: Two-dimension whispering gallery mode of light within a PANDA ring waveguide in GaAsP/InP, where (a) PANDA ring radius is 4.5 µm, the left-right ring radii are 1.55 µm, (b) the WGM output of waveguide with wavelength 1.892 µm, (c) the Through port signal, (d) the Drop port signal with frequency between 1-300 THz.

In this work, the simulations based on practical software called Opti-wave FDTD and MATLAB programs were chosen [63], where a 100 fs Gaussian pulse is modulated by a 200 THz carrier and incident via the PANDA ring input port into the artificial eye model. The waveguide thickness and material composition is considered by computing the effective refractive index, n_{eff}, for the fundamental mode at λ= 1.55 µm. In the vertical direction, each waveguide structure is 0.45 µm thick, with vertical core thicknesses of 0.3 µm to 0.5 µm, and the n_{eff} value are between 3.2 and 3.4. The parameters are obtained by using the practical material parameters, where the used material is an InGaAsP/InP. Therefore, the waveguide core, with refractive index n_1=3.14, is bordered on each side by air (n_2.=1). The add-drop optical multiplexer and the side ring parameters of the three cascade ring radii are R_1=R_2=3µm, the center ring radius is R_3=1µm. The coupling coefficient coefficients are $\kappa_1 = \kappa_2 = \kappa_3 = \kappa_4 = \kappa_5 = \kappa_6 = 0.5$, where the effective core area of the waveguides is A_{eff} =0.25 µm^2, and the waveguide, loss coefficient is α = 0.1 dBmm^{-1}. In this article, the experimental results are achieved by using the WGM result is obtained by Opti-wave as shown in Fig. 5(a). The WGMs depend on the used parameters and conditions, where the other input signals can be modulated by the ADD port input signals. A pixel of artificial vision is designed to produce the 3D images where the image (data signal) can be transmitted by modulating the signal amplitude of the various wavelengths. As you can see from Fig. 5, the proposed system is a micro scale device, which is about 14 µm, which is around human hair dimension. Such a tiny device can be embedded within the eyes without damaging the other cells. In application, the WGM signals can be generated and controlled, for instance; the WGM switching signals can be selected to the required directions, i.e. switching up or down direction, which can be useful for 3D image information connection as shown in Fig. 5(b), where the image information is constructed and represented by WGM, which is then connected by focusing beam, i.e. WGM switching control, to the optic nerve cells and chiasm as shown in Figs. 5(a) and 5(b).

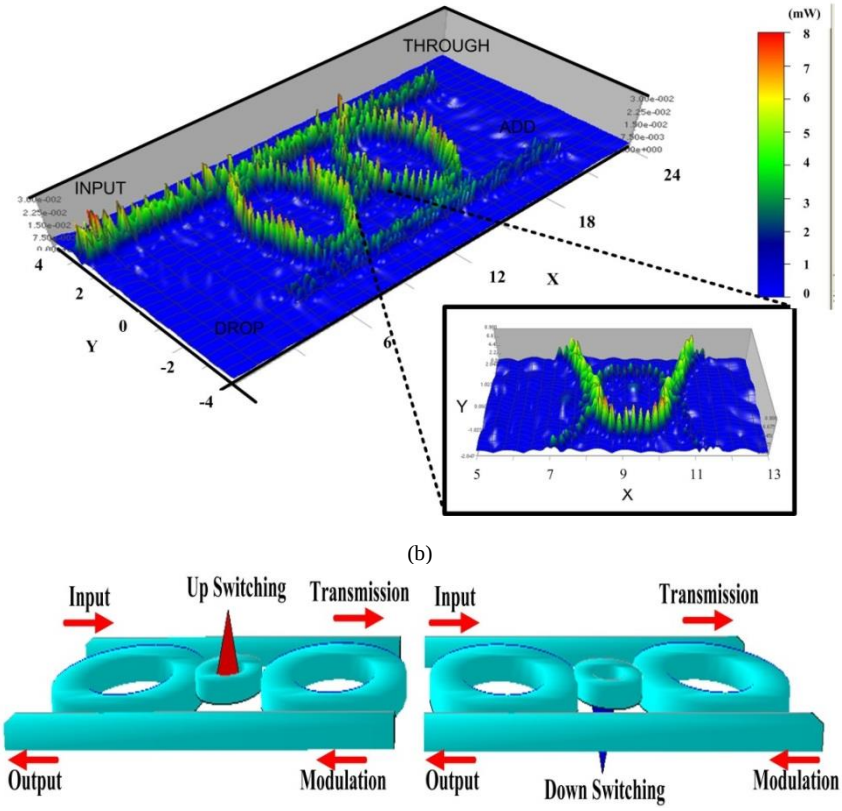


Fig. 5. Schematic of WGM switching signals, where (a) 3D whispering gallery mode of light within a waveguide, (b) the switching signals (Up or Down) can be controlled using the modulated signal input.

4. Conclusion

In this paper, the novelty is that the 3D image construction can be obtained using the micro-ring resonator system, which is known as a Panda ring resonator, from which the 3D pixel imaging can be generated and realized. However, this is a simulation work, in which all device parameters were chosen closely to the practical device parameters that can be fabricated by the present fabrication technology. The analytical solution of WGM within the proposed system is also given. In application, the large area of pixels can be formed and embedded as a thin-film device, which can be used to form the large image information. This method can be used to form the artificial eyes, where the human eyes can be operated, and the artificial perception (vision) realized. The spying imaging construction and re-construction of 3D imaging vision cam also be available by using the invisible light wavelength, which can be used for security purpose.

5. Acknowledgments

The author would like to give the acknowledgement to King Mongkut's Institute of Technology Ladkrabang (KMITL), Bangkok 10520, Thailand for the research laboratory facilities.

References

[1] J.D. Weiland and M.S. Humayun, "Intraocular retinal prosthesis," IEEE Engineering in Medicine and Biology Magazine October: 60-66(2006). http://dx.doi.org/10.1109/MEMB.2006.1705748.

[2] K. H. Jeong, J. Kim and L. P. Lee "Biologically inspired artificial compound eyes", Science, 312(57773): 557 -561 (2006). http://dx.doi.org/10.1126/science.1123053.

[3] Q. He, J. Liu, B. Yang, Y. Dong, C. Yang, "Fabrication and characterization of biologically inspired curved-surface artificial compound eyes," J. Microelectronical System, 22 : 4-6 (2013). http://dx.doi.org/10.1109/JMEMS.2012.2226934.

[4] W.H. Dobelle, "Artificial vision for the blind by connecting a television camera to the visual cortex," ASAIO J 46: 3–9(2000). http://dx.doi.org/10.1097/00002480-200001000-00002.

[5] E. Kaniusas, G. Varonecka, B. Mahr, C. Szeles, "Optic visualization of auricular nerves and blood: optimization and validation," Instrumentation and Measurement, Transaction on 60:3253-3258(2011). http://dx.doi.org/10.1109/TIM.2011.2159314.

[6] K. Tamee, K. Chaiwong, K. Yothapakdee and P.P Yupapin, "Brain signal monitoring and encoding for humanoid robots use," J. Biosensors & Bioelectronics 4:13e-124(2013).

[7] J.B. Jonas, A.M. Schmidt, J.A. Müller-Bergh, U.M. Schlötzer-Schrehardt, and G.O. Naumann, "Human optic nerve fiber count and optic disc size". Investigative Opthalmology & Visual Science, 33: 2012-2018(1992).

[8] J.B. Jonas, P. Martus, F.K. Horn, A. Jünemann, M. Korth, and W.M. Budde, "Predictive factors of the optic nerve head for the development of progression of glaucomatous visual field loss," IOVS Investigative Ophtalmology & Visual Science, 45:2613-2618(2004). http://dx.doi.org/10.1167/iovs.03-1274.

[9] G.M. Cavallini et al., "Optic nerve aplasia and microphthalmos: a case report," J. Genetic Syndromes & Gene Therapy 4: 000175(2013). http://dx.doi.org/10.4172/2157-7412.1000175.

[10] F.D. Zainol, N. Thammawongsa, S. Mitatha, J. Ali and P.P. Yupapin, "Nerve communication model by bio-cells and optical dipole coupling effects," Artificial Cells, Nanomedicine and Biotechnology, 2013: 1-8(2013). http://dx.doi.org/10.3109/21691401.2012.759124.

[11] K. Tamee, K. Chaiwong, K. Yothapakdee and P.P. Yupapin, "Psychiatric investigation using WGMs using a nonlinear microring circuit," J Innovative Optical Health Sciences, 6: 1-8 (2013). http://dx.doi.org/10.1142/S1793545813500442.

[12] K. Uomwech, K. Sarapat and P.P. Yupapin, "Dynamic modulated Gaussian pulse propagation within the double PANDA ring resonator", Microw. Opt. Technol. Lett., 52: 1818-1821(2010). http://dx.doi.org/10.1002/mop.25315.

[13] P.P. Yupapin, "Nonlinear coupling effects of waves in a panda ring," Science Discovery 1: 1-5(2013). http://dx.doi.org/10.11648/j.sd.20130101.11.

[14] N. Sarapat, T.D. Frank and P.P. Yupapin, "Conjugate mirror design and simulation using a nonlinear coupling microring circuit," J Nonlinear Optical Physics & Materials, 23(4): 1-11(2013). http://dx.doi.org/10.1142/s0218863513500240.

[15] H.H. Lund, "Modern artificial intelligence for human-robot interaction", IEEE Proceeding, 92(11): 1821-1838 (2004). http://dx.doi.org/10.1109/jproc.2004.835362.

[16] M.J. Mataric, "Using humanoid robots to study human behavior," IEEE Intelligent System and their Applications, 15(4): 46-56(2000). http://dx.doi.org/10.1109/5254.867912.

[17] J. Sinapov, V. Sukhoy, R. Sahai, A. Stoytchev, "Vibrotactile recognition and categorization of surfaces by a humanoid robot," Robotics, IEEE Transaction on, 27(3), 488-497(2011). http://dx.doi.org/10.1109/TRO.2011.2127130.

[18] K. Kuang, M. Gibson, B.E. Shi, M. Rucci, "Active vision during coordinated head/eye movements in a humanoid robot," IEEE Robotics, Transaction on, 28(6):1423-1430(2012). http://dx.doi.org/10.1109/TRO.2012.2204513.

[19] K. Yokoi, N. Kawauchi, N. Sawasaki, T. Nakashima, S. Nakamura, Y. Yanagihara, K. Sawada, I. Takeuchi, K. Nakashima, Y. Yanagihara, K. Yokoyama, T. Isozumi, Y. Fukase, K. Kaneko, H. Inoue, "Humanoid robotics applications in HRP," International Journal of Humanoid Robotics, 1(3): 409-428(2004). http://dx.doi.org/10.1142/S0219843604000265.

[20] E. Torta, H.R. Cuijpers, J.F. Juola, D. Van Der Pol, "Modeling and testing proxemic behavior for humanoid robots", International Journal of Humanoid Robotics, 9(4): 1250028-24(2012). http://dx.doi.org/10.1142/S0219843612500284.

[21] M. Xie, "Five Steps of evolution from non-life to life-like robot," International Journal of Humanoid Robotics, 6(2), 307-327(2010). http://dx.doi.org/10.1142/S0219843609001759.

[22] P. Coiffet, "An introduction to bio-inspired robot design," International Journal of Humanoid Robotics, 2(3): 229-276(2005). http://dx.doi.org/10.1142/S0219843605000533.

[23] A. Bauer, D. Wollherr, M. Buss, "Human robot collaboration: A survey," International Journal of Humanoid Robotics, 5(1): 47-66(2008). http://dx.doi.org/10.1142/S0219843608001303.

[24] P. Patel, "The brain-machine Interface: Unplugged," IEEE Spectrum, 46(10): 13-14(2009). http://dx.doi.org/10.1109/MSPEC.2009.5267979.

[25] P.Y. Han, G. C. Cho, and X. C. Zhang, "Time-domain trans-illumination of biological tissues with terahertz pulses," Opt. Lett., 25: 242-244(2000). http://dx.doi.org/10.1364/OL.25.000242.

[26] S.W. Smye, J. M. Chamberlain, A. J. Fitzgerald, and E. Berry, "The interaction between terahertz radiation and biological tissue," Phys. Med. Biol., 46: 101-112(2001). http://dx.doi.org/10.1088/0031-9155/46/9/201.

[27] E. Pickwell and V. P. Wallace, "Biomedical applications of terahertz technology," J. Phys. D: Appl. Phys., 39: 301-310(2006). http://dx.doi.org/10.1088/0022-3727/39/17/R01.

[28] J.-H.Son, "Terahertz electromagnetic interactions with biological matter and their applications," J. Appl. Phys., 105, Art No: 102033(2009). http://dx.doi.org/10.1063/1.3116140.

[29] R.M. Woodward, B. E. Cole, V. P. Wallace, D. D. Arnold, R. J. Pye, E. H. Linfeld, M. Pepper, and A. G. Davies, "Terahertz pulse imaging of in vitro basal cell carcinoma samples," TOPS, 56: 329-330(2001). http://dx.doi.org/10.1109/cleo.2001.947872.

[30] R.M. Woodward, B. E. Cole, V. P. Wallace, R. J. Pye, D. D. Arnold, E. H. Linfield, and M. Pepper, "Terahertz pulse imaging in rejection geometry of human skin cancer and skin tissue," Phys. Med. Biol., 47: 3853-3863(2002). http://dx.doi.org/10.1088/0031-9155/47/21/325.

[31] H. Lee, D.S. Lee, H. Kang, B.-N. Kim, M.K. Chung, "Sparse brain network recovery under compressed sensing," Medical Imaging, IEEE Transaction on, 30(5): 1154-1165(2011). http://dx.doi.org/10.1109/TMI.2011.2140380.

[32] M. Milev, M. Hristov, "Analog implementation of ANN with inherent quadratic nonlinearity of the synapses," Neural networks, IEEE Transaction on, 14(5): 1187-2000(2003).

[33] E. Pickwell, B. E. Cole, A. J. Fitzgerald, M. Pepper, and V. P. Wallace, "In vivo study of human skin using pulsed terahertz radiation," Phys. Med. Biol., 49: 1595-1607(2004). http://dx.doi.org/10.1088/0031-9155/49/9/001.

[34] V.P. Wallace, A. J. Fitzgerald, E. Pickwell, R. J. Pye, P. F. Taday, N. Flanagan, and H. A. Thomas, "Terahertz pulsed spectroscopy of human basal cell carcinoma," Appl. Spectroscopy, 60: 1127-1133(2006). http://dx.doi.org/10.1366/000370206778664635.

[35] E. Pickwell, B. E. Cole, A. J. Fitzgerald, V. P. Wallace, and M. Pepper, "Simulation of terahertz pulse propagation in biological systems," Appl. Phys. Lett., 84: 2190-2192(2004). http://dx.doi.org/10.1063/1.1688448.

[36] M.A. Jalil, A. Abdolkarim, T. Saktioto, C.T. Ong, P.P. Yupapin, "Generation of THz frequency using PANDA ring resonator for THz imaging, imaging," International Journal of Nanomedicine, 7: 773 – 779(2012).

[37] C.W. Gillian, E. Berry, S.W. Smye, N.N. Zinov'ev, A.J. Fitzgerald, R.E. Miles, M.C. and M. A. Smith, "Modeling the propagation of terahertz radiation through a tissue simulating phantom", Physics of Medicine and Biology, 49:1853-1864(2004). http://dx.doi.org/10.1088/0031-9155/49/10/002.

[38] D.Y. Heh and E.L. Tan, "Modeling the interaction of terahertz pulse with healthy skin and basal cell carcinoma using the unconditionally stable fundamental ADI-FDTD method", Progress In Electromagnetics Research B, 37: 365-386(2012). http://dx.doi.org/10.2528/PIERB11090905.

[39] I.S. Amiri and J. Ali, Deform of biological human tissue using inserted force applied by optical tweezers generated by PANDA ring resonator, *Quantum Matter*, 3:24-28(2014). http://dx.doi.org/10.1166/qm.2014.1091.

[40] S. E. Alavi et al., Generation of femtosecond soliton tweezers using a half-Panda system for modeling the trapping of a human red blood cell. *Journal of Computational and Theoretical Nanoscience* (JCTN), 12:10-18(2015). http://dx.doi.org/10.1166/jctn.2015.3689.

[41] I.S.Amiri, A. Afroozeh and H. Ahmad. *Integrated micro-ring photonics: Principles and Applications as Slow light devices, Soliton generation and Optical transmission*, CRC Press, (2015).

[42] I. S. Amiri, J. Ali, Nano particle trapping by ultra-short tweezer and wells using MRR interferometer system for spectroscopy application. *Nanoscience and Nanotechnology Letters*, 5(8): 850-856, (2013). http://dx.doi.org/10.1166/nnl.2013.1636.

[43] I.S. Amiri and J. Ali, Nano optical tweezers generation used for heat surgery of a human tissue cancer cells using Add/Drop interferometer system. *Quantum Matter*, 2, 489-493, (2013). http://dx.doi.org/10.1166/qm.2013.1087.

[44] I.S. Amiri and J. Ali, Optical buffer application used for tissue surgery using direct interaction of nano optical tweezers with nano cells. *Quantum Matter*, 2, 484-488, (2013). http://dx.doi.org/10.1166/qm.2013.1086.
[45] I. S. Amiri et al., Optical stretcher of biological cells using sub-nanometer optical tweezers generated by an Add/Drop microring resonator system, *Nanoscience and Nanotechnology Letters*, 6, 111-117, (2014.)
[46] I.S. Amiri, A. Nikoukar, Ali, J. et al., Ultra-short of pico and femtosecond soliton laser pulse using microring resonator for cancer cells treatment, *Quantum Matter*, 1, 159-165, (2012). http://dx.doi.org/10.1166/qm.2012.1015.
[47] N. Thmmawongsa and P.P. Yupapin, Remote artificial eyes using micro-optical circuit for long-distance 3D imaging perception, Artificial Cells, Nanomedicine and Biotechnology, 2014, 1-5(Early accessed), (2014).
[48] N. Thammawongsa N, J. Ali and P.P. Yupapin, Artificial vision model by small scale conjugate mirrors, Journal of Biosensors and Bioelectronics, 4:e125, 2014.
[49] D. Deng and Q Guo, Ince-Gaussian solitons in strongly nonlocal nonlinear media. Opt. Lett., 32(2), 3206-3208, (2007). http://dx.doi.org/10.1364/OL.32.003206.
[50] I. Srithanachai, S. Ueamanapong, S. Niemcharoen, S. & Yupapin, P. P., Novel design of solar cell efficiency improvement using an embedded electron accelerator on-chip. Opt. Express, 20(12), 12641-12642, (2012). http://dx.doi.org/10.1364/OE.20.012640.
[51] Y. Kokubun, Y. Hatakeyama, M. Ogata, S. Suzuki and N. Zaizen, Fabrication technologies for vertically coupled micro ring resonator with multilevel crossing busline and ultracompact-ring radius. IEEE J. Sel. Top. Quant. Electron, 2005, 11(1), 4–10, (2005).
[52] J. Jin, the Finite Element Method in Electromagnetic. 2nd edition. NJ, Wiley, 2010.
[53] K. Kawano and T. Kitoh, Introduction to Optical Waveguide Analysis Solving Maxwell's Equations and the Schrodinger Equation. New York: John Wiley, (2001). http://dx.doi.org/10.1002/0471221600.
[54] J.C. Knight, N. Dubreuil, V. Sundoghdar, J. Hare, V. Lefevre, J.M. Raimond and S. Haroche, Characterizing whispering-gallery mode in microspheres by direct observation of the optic standing-wave pattern in the near field. Opt. Lett., 21(10), 698-670, (1996). http://dx.doi.org/10.1364/OL.21.000698.
[55] H. Quan and Z. Guo, Analyses of whispering-gallery modes in small resonators. J. Micro. Nanolith. Mems, 8(3), 033060-3, (2009). http://dx.doi.org/10.1117/1.3213247.
[56] J. Hu and C.R. Menynk, Understanding leaky modes: slab waveguide revisited. Advance in Optic and Photonices 1, 58(2), 63-70, 2009.
[57] J.D. Jackson, Classical Electrodynamics. 2 nd edition, New York: John Wiley & Sons, (1962).
[58] V. Zakharov, Lecture Notes Bessel Function and their Applications to Solution of Partial Differential Equation. New York: Vanderbilt University Press, 2009.
[59] E. Schechter, Cubic Formula. [Online] Available from: http://www.math.vanderbilt.edu/.../cubic/.html. [Accessed: March 2015].
[60] P.P. Yupapin and P. Suwancharoen, Chaotic signal generation and cancellation using a micro ring resonator incorporating an optical add/drop multiplexer. Opt. Commune, 280(2), 343–350, (2007). http://dx.doi.org/10.1016/j.optcom.2007.08.018.
[61] Z. Guo, H. Quan and S. Pau, Numerical characterization of whispering-gallery mode optical microcavities. Appl. Opt., 45(4), 611–618, (2006). http://dx.doi.org/10.1364/AO.45.000611.
[62] H. Quan and Z. Guo, Analyses of whispering-gallery modes in small resonators. J. Micro. Nanolith. Mems. Moems, 8(3), 033060, 2009. http://dx.doi.org/10.1117/1.3213247.
[63] OptiFDTD by Opti-wave Corporation Company, Version 8.0, single license, (2008).